Universidad Zaragoza

Master thesis
Máster en física y tecnologías físicas

Rocksalt ionic insulators for atomic scale ferroelectrics

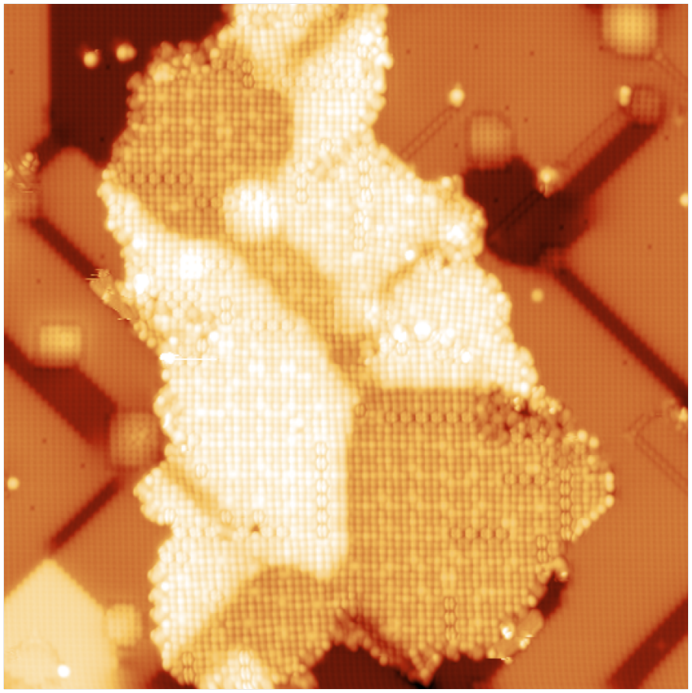

Sonja Schubert
supervised by
Dr. David Serrate and Dr. Marten Piantek
Instituto de Nanociencia de Aragón

September 15, 2016

Contents

Introduction

Today's electronic devices have already reached sizes close to the atomic scale. Information storage based on magneto-resistive devices is the most common technique, but it is rapidly approaching the superparamagnetic limit of several nm domain size at room temperature. Therefore alternative methods have to be taken into account, one of them are ferroelectric-based devices. The bistable polarization in such materials can be exploited in digital technologies similarly to magnetic polarization. In contrary to ferromagnetic domain size, the critical thickness for these materials is not yet explored[1].
Ferroelectricity at atomic scale has been shown recently in ultrathin layers of NaCl on $Cu_2N/Cu(001)$, see fig.1. A strain-induced out-of-plane electric dipole in NaCl bilayer islands can be controlled by an external electric field between tip and sample in a Scanning Probe Microscope (SPM)[2]. The polar insulator Cu_2N plays an important role to enable the tuning of the polarization direction. It causes the electronic decoupling of the binary rock salt compound from the Cu(001) surface. It also allows the breaking of the inversion symmetry. Therefore a spontaneous polarization at zero electric field can be found for $NaCl/Cu_2N$.

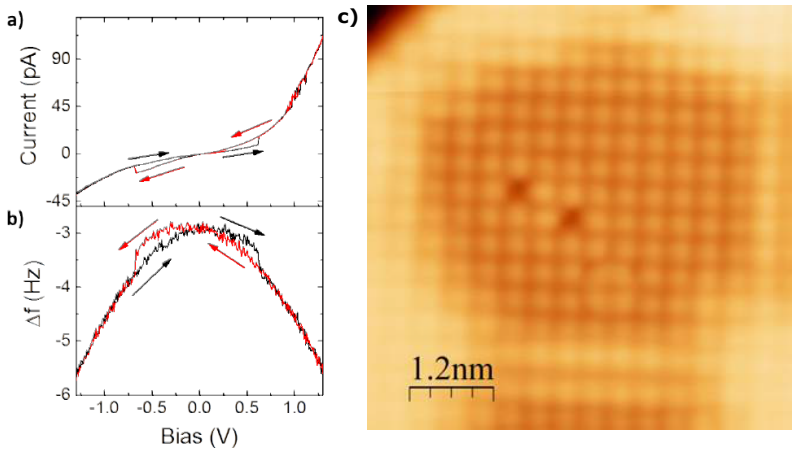

Figure 1: *Ferroelectricity in NaCl bilayer islands on $Cu_2N/Cu(001)$ near a vacancy a) I(V)-curve with characteristic hysteresis and two sharp steps b) $\Delta f(V)$-spectroscopy with two parabolas for the two different polarization states, c) STM topography of a NaCl bilayer island on $Cu_2N/Cu(001)$ showing two vacancies (V_{bias}=-1.3V, I=50 pA)[1]*

To explore the role of epitaxial strain, other binary rock salts with different lattice mismatch relative to $Cu_2N/Cu(001)$ were investigated in this thesis. Since an in-plane strain is associated to the rumpling perpendicular to the surface of the outtermost layer, it was expected to increase the polarization due to larger lattice mismatchs and therefore to affect strongly the ferroelectric

behaviour.

Two binary rock salts with different lattice parameter with respect to NaCl (bulk lattice parameter: 0.564 nm) were selected: LiCl, with a bulk lattice parameter of 0.514 nm and KBr, with 0.6586 nm [1].

LiCl was sucessfully grown on Cu(001) and Cu_2N/Cu(001). On Cu(001) no sizeable strain can be found due to identical lattice parameters, but on Cu_2N/Cu(001) LiCl adopts the lattice parameter of the substrate and grows with small strain. Due to the relative small lattice mismatch with respect to Cu(001) and Cu_2N/Cu(001) the investigation of the ferroelectric properties of KBr were given priority in this thesis.

Surprisingly it was found that KBr-BL/Cu_2N/Cu(001) even growing unstrained with its own bulk lattice parameter, still showed a bistable ferroelectric behaviour. Therefore out-of-plane dipoles are induced also without strain-forced rumpling, contrary to the assumption from the measurements of NaCl-BL/Cu_2N/Cu(001).

For KBr/Cu(001) an electronic superstructure due to the periodic variation of the dipole moments with the structural Moiré was found. The interaction between Cu(001) and KBr gives rise to in-gap-states. On Cu_2N/Cu(001) these in-gap-states are suppressed due to the intercalated insulating layer, but the conduction band edge and the interface state of Cu_2N/Cu(001) can be also observed in the KBr adlayers. The workfunctions on the different substrates could be measured with I (z)-spectroscopy and an other method based on field emission resonances. In this thesis we applied the following experimental techniques: Scanning Tunneling Microscopy(STM), Scanning Tunneling Spectroscopy(STS), Atomic Force Microscopy(AFM), Kelvin-Probe-Spectroscopy and Low Energy Electron Refraction(LEED).

1. Experimental techniques

1.1. Scanning tunneling microscopy (STM)

Scanning tunneling techniques are based on the quantum mechanical tunneling effect. A conducting tip is placed a few angström above a conducting or semiconducting sample as shown in fig.2a). Given the work functions of tip and sample, the vacuum gap represents a potential barrier, through which the electrons can tunnel quantum mechanically in both directions.

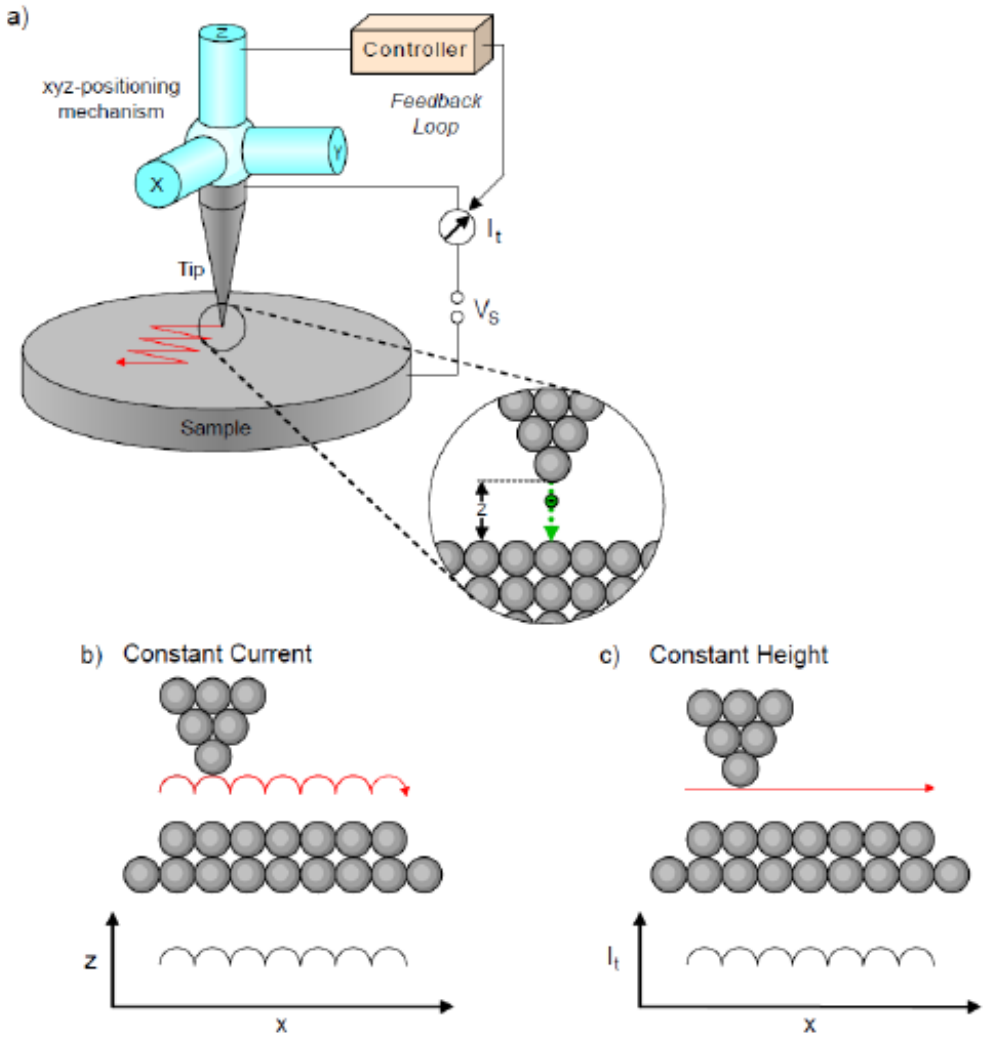

Figure 2: *Schematic setting of a STM: Between sample and tip a bias voltage is applied, the measured trajectory is indicated by the red line (a)) and the two scanning modes: constant current (b)), the tunneling current is kept constant while z is recorded, and constant height (c)), where z is kept constant and information can be get out of the tunneling current measured in each point, figure from [4]*

In the 1D approximation of plane waves, squared potential barrier and small sample bias, the tunneling current depends on the tip-sample distance z as follows:

$$I(z) = I_0 \exp(-2kz) \tag{1}$$

with

$$k = \frac{\sqrt{2m\left(\frac{\phi_{tip}+\phi_{sample}}{2}\right)}}{\hbar} \tag{2}$$

where ϕ_{tip} and ϕ_{sample} are the work functions of the indicated materials.
Two scanning modes are commonly used: **Constant height** and **constant current mode**.
With the **constant current mode** high corrugations can be measured. The tunneling current is kept constant and the height z is regulated due to a feedback-loop, see fig.2b).
In the **constant height mode** the tip is held at the same height z during scanning laterally over the surface and the change of the tunneling current is measured, see fig.2c). The advantage of this mode is the possiblility to measure also small currents and the disentanglement of feedback crosstalk with electronic properties of the surface. The disadvantage is that roughness of the sample surface can cause direct contact of the tip with the sample and therefore a change of the tip apex and the measurement conditions and the alteration of the sample.
In both cases, the resulting information carries the electronic structure of the sample surface. Information about the geometric structure can be obtained with atomic force microscopy, see section 1.6.

1.2. Scanning tunneling spectroscopy (STS)

Scanning tunneling spectroscopy is used to investigate the electronic structure by measuring the local density of states (LDOS) of a certain point (x,y) of the surface. The differential tunneling conductance dI(V)/dV measured using a lock-in-amplifier is proportional to the sample LDOS[23]:

$$\frac{dI(V,x,y)}{dV} \propto \rho_s(E = eV, x, y) \tag{3}$$

with E the electron energy referenced to the sample's Fermi level.
By scanning slowly over a surface area, it is possible to measure the dI(V)/dV signal in every image point at a certain energy eV_{bias}, which results in a spatially resolved LDOS map (a dI/dV map) of the scanned area.

1.3. Surface dipole moment

The work function ϕ of a surface is proportional to the surface dipole moment μ [7]. A larger decay length of the bulk's charge density into de vacuum corresponds to a higher surface dipole

moment and therefore a higher work function:

$$\mu = -\frac{\phi A}{4\pi} \tag{4}$$

with A the surface area. Conducting surfaces should exhibit a larger workfunction than insulators[1].

1.4. I(z)-spectroscopy

During the acquisiton I(z) curves, the tip height z towards the sample is changed and the tunneling current I is recorded. With equation (1) and (2) it is possible to calculate the average work function $\phi_{average} = \frac{\phi_{tip}+\phi_{sample}}{2}$ of tip and sample by fitting the I(z) curve to an exponential behaviour. Therefore the work function depends not only on the sample, but also on the tip. The tip is assumed to be metallic, and therefore a higher workfunction than for the insulating materials is expected. This leads to a higher workfunction average than the workfunction value only for the insulating adlayers.
I(z)-spectroscopy is sensitive to elastic deformation of the surfaces, which can occur during approaching the tip towards the sample and hinder the value of $\phi_{average}$[9]. Because of this disadventage it is not possible to measure close to the sample and therefore the resulting workfunction is only a average over a certain area of the surface. The results of this method depend also on the applied bias voltages. A uncertainty of approximatly 1 eV was found here between a bias voltage of -1.3 V and 1.4 V.

1.5. Field emission resonances (FER)

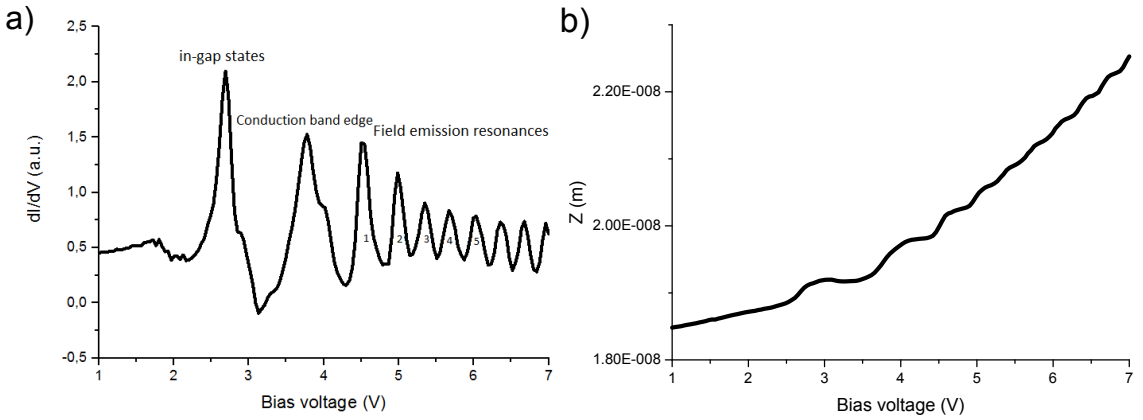

Figure 3: *Field emission resonance measurements on KBr-Ml-Island on Cu(001) (closed feedback), a) dI/dV(V)-curve and b) z(V)-curve*

In fig.3 a STS curve and the corresponding z(V)-curve taken on KBr-ML/Cu(001) are shown. Above 4.2 V field emmision resonances (FER) can be observed.
When the applied bias voltage between tip and sample exceeds the work function of the sample, electrons are able to enter into the vacuum gap. Tip and sample form a quantum well and the free electrons are reflected at the potential walls. Therefore standing waves which are the eigenstates of this quantum well can be observed as a large number of resonances states for $V_{bias}>\phi$ in STS measurements. With the approach of a 1D potential between tip and sample and that only higher resonances are taken into account, the FER energies are given by[8]:

$$eV_n = \phi + \left(\frac{3\pi\hbar e}{2\sqrt{2m}}\right)^{2/3} E^{2/3} n^{2/3} \tag{5}$$

with e the electron charge, ϕ the work function of the surface, m the electron mass, n the number of the resonance, E the electric field and V_n the voltage of the nth resonance. The FER are recorded closed feedback and due to the z-position-readjustment to keep the current constant, the electric field can be calculated with the approximation of the parallel plate capacitor model:

$$E = \frac{V_{bias}}{z} \tag{6}$$

In contrast to the I(z)-spectroscopy, FER-measurement are more local[8] and the resulting work-functions are smaller due to the direct measurement of the workfunctions of the sample.

1.6. Non-contact atomic force miscroscopy (nc-AFM)

The working principle of a nc-AFM consists in the interaction between tip and sample in form of different forces. A schematic setting of the STM/AFM is shown in fig.4. The motion of a oscillating cantilever can be described by a driven harmonic oscillator[3]:

$$m\ddot{z} - \frac{m\omega_0}{Q}\dot{z} + k_0 x = F_D \cos\omega t \tag{7}$$

with m the effective mass, F_D the driving force, Q the quality factor, ω_0 the resonance frequency and k_0 the spring constant of the oscillator.
The vacuum resonance frequency is given by:

$$f_0 = \frac{\pi}{2}\sqrt{\frac{k_0}{m}} \tag{8}$$

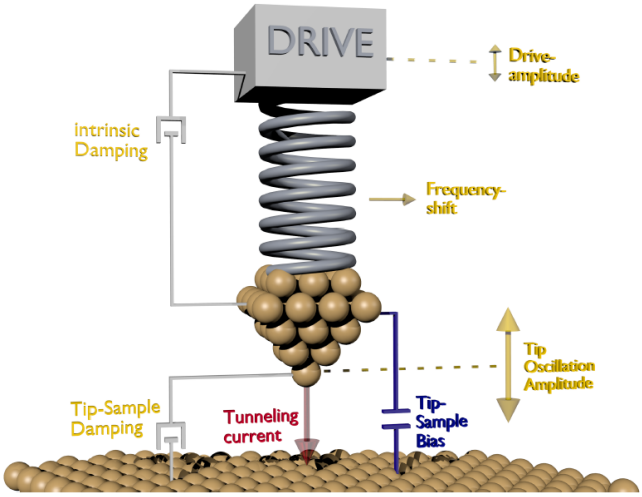

Figure 4: *Schematic setting of a STM/AFM, indicated with yellow letters are the observables from the AFM part, figure from [3]*

The cantilever is affected by different forces F_{TS} between tip and sample when brought close to the sample. The force gradient changes the effective stiffness on the cantilever and therefore a detuning to a new resonance frequency occurs:

$$f' = \sqrt{\frac{k_0 - \frac{\partial F_{TS}(z)}{\partial z}}{m}} \tag{9}$$

The frequency shift Δf is defined as the difference between the vacuum resonance frequency and the resonance frequency due to sample-cantilever interaction:

$$\Delta f = f_0 - f' \tag{10}$$

For small oscillation amplitudes the frequency shift $\Delta f(z)$ can be written as:

$$\Delta f(z) = -\frac{f_0}{2k_0}\frac{\partial F_{TS}}{\partial z} \tag{11}$$

Therefore it is proportional to the gradient of the force between tip and sample.
With this technique, in contrary to the STM also insulating surfaces can be measured. Nowadays quartz oscillators can be used instead of conventional AFM cantilevers. These sensors offer a higher stiffness and the piezoelectric material gives a direct electronic readout of the mechanical oscillation. This allows to operate them at oscillation amplitudes in the range of tens of pm and make them hence sensitive to chemical forces. Furnished with an STM tip, electronic and structural properties can be measured simultaneously.

1.7. Interaction forces

- **Chemical forces** due to overlapping of the orbitals, which are normally described by the Lennard-Jones-Potential

$$E_{LJ} = \epsilon \left(\left(\frac{z_m}{z} \right)^{12} - 2 \left(\frac{z_m}{z} \right)^{6} \right) \tag{12}$$

with z_m the equilibrium distance and ϵ the potential depth. The first term describes the Pauli repulsion due to the overlap of filled orbitals at short distances, the second term includes attracting chemical forces. To obtain the chemical forces in z-direction, the Lennard-Jones Potential is differentiated with respect to z:

$$F_{chem}(z) = -\frac{\delta E_{LJ}}{\delta z} = \frac{12\epsilon}{z_m} \left(\left(\frac{z_m}{z} \right)^{13} - 2 \left(\frac{z_m}{z} \right)^{7} \right) \tag{13}$$

- **Van-der-Waals forces (vdW)**, with the origin in induced and permanent dipol-dipol interaction. In the approach by Hamaker [6] for the case of a sphere with radius R with distance z to an infinite plane the interacting force is given by:

$$F_{vdW}(z) = -\frac{HR}{6z^2} \tag{14}$$

with H the Hamaker constant depending on the material. Therefore the vdW force in this case is proportional to the radius of a sphere and in the case of the AFM of the tip apex, which makes a sharp tip crucial to decrease the influence of the vdW forces.

- **Electrostatic forces** due to the potential difference between tip and sample. In a first approach the model of a parallel plate capacitador can be used[24]:

$$F_{el} = -\frac{\delta E_{cap}}{\delta z} = \frac{1}{2} \frac{\partial C}{\partial z} V_{eff}^2 \tag{15}$$

with E_{cap} the energy stored in the capacitor and C the capacitance of the capacitor. The effective electrostatical potential V_{eff} is contributed by the external applied bias voltage V_{bias} and the contact potential difference CPD:

$$V_{eff} = V_{bias} + CPD \tag{16}$$

1.8. Δf(V)-spectroscopy and Δf(z)-spectroscopy

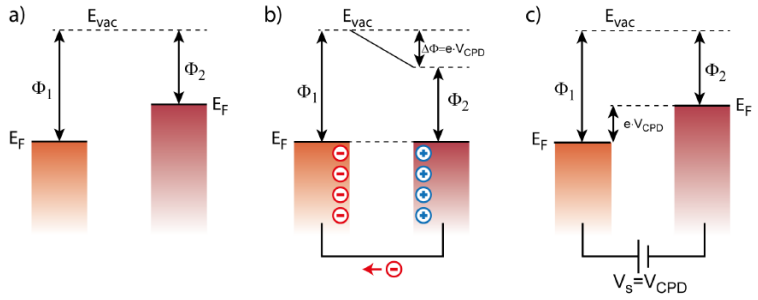

Figure 5: *Contact potential difference: Two metals with different work functions $\|\phi_1\| > \|\phi_2\|$ a) without electrical contact: their vacuum levels are aligned, b) when brought in contact, the chemical potential equal, and a negative charge transfer into the metal with the higher workfunction takes place, c) therefore the contact potential difference occurs figure from [3]*

In fig. 5 two metals with different work functions are shown. First, when they are separated, they have the same vacuum level, see fig.5a), but when they are brought in electrical contact, their Fermi levels will align, see fig.5b). Therefore electrons will move from the metal with the lower work function to the metal with the higher work function and the so-called contact potential difference can be observed:

$$CPD = \frac{\phi_2 - \phi_1}{e} \tag{17}$$

e the elementary charge of the electron, see fig.5c).

When the tip is placed over a fix point of the surface and Δf is recorded in dependence of the ramped bias voltage V_{bias}, the force gradient in the capacitor approach can be written as[5] (see eq.(15)):

$$\Delta f(V_{bias}) \propto -\frac{\delta F}{\delta z} = -\frac{1}{2}\frac{\delta^2 C}{\delta z^2}(V_{bias} + CPD)^2 + \Delta f \tag{18}$$

Therefore $\Delta f(V_{bias})$ is a parabola with the maximum (see fig.6b)) centered in the value of the contact potential difference (CPD), the slope $\frac{\delta^2 C}{\delta z^2}$ shows the distance-dependence capacitance. The Δf offset of the Δf(V)-spectroscopy curve corresponds to the Lennard-Jones Potential, the VdW forces, Pauli interaction and the chemical interactions. If the tip is brought closer to the surface, the offset will be shifted to more negative values due to stronger vdW interaction, if the regime of Pauli repulsion is not already reached. The voltage of the maxima of the parabola describes the local contact potential difference LCPD.

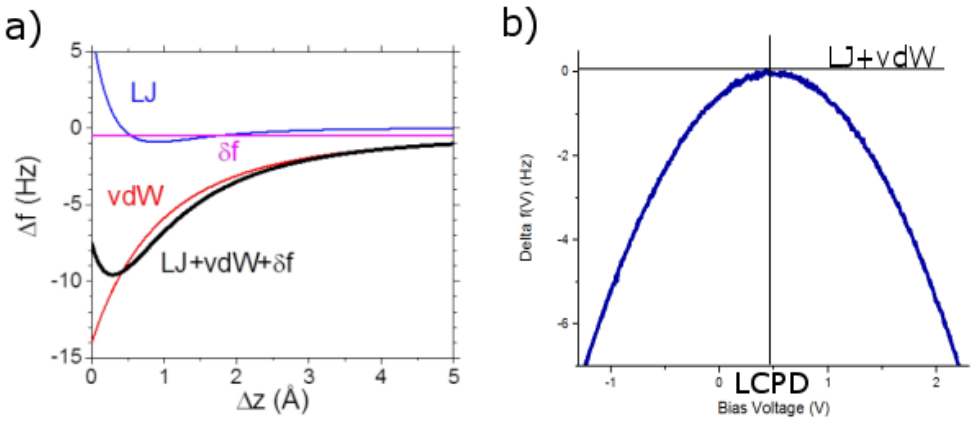

Figure 6: *Interacting forces between tip and sample in a) $\Delta f(z)$-spectroscopy[18] and b) $\Delta f(V)$-spectroscopy (Kelvin-Probe): Lennard-Jones Potential with Pauli repulsion and chemical forces LJ, electrostatic forces δf (eq.(18)), van-der-Waals forces vdW, local contact potential difference LCPD*

In fig.6a) Δf(z)-spectroscopy is displayed with its components: the vdW- and chemical forces and the Pauli repulsion. The offset with week distance dependence corresponds to the electrostatical forces.

1.9. Ferroelectricity

A material is called ferroelectric if it shows two or more stable or metastable electric polarization P states. These states are separated by a finite energy barrier, which can be overcome by a applied external electric field and therefore a switch between the different states are possible[1]. The electrical polarization of a ferroelectric material is defined by[9]:

$$\vec{P} = \chi_E \epsilon_0 \vec{E} + \vec{P}_0 \tag{19}$$

With χ_E the electrical suscepility, E the electrical field in the material and P_0 the polarization at zero electric field. The arrangement of the ions in the crystal lattice of a ferroelectric material does not allow a perfect dipole compensation. Therefore also at zero electric field a finite polarization can be found. In conventional ferroelectric films, this state results from a spontaneous breaking of the lattice inversion symmetry below the ordering temperature.

1.10. Experimental details

For cleaning the Cu(001) crystal sputtering (with Ar ions (1 keV)) and annealing (873 K) cycles were used. KBr (LiCl) was deposited after cooling down the sample to approximatly room temperature. The deposition of KBr(LiCl) was performed with a Knudsen efussion cell operated at 728 K (628

K).
For the preparation of KBr (LiCl)/Cu_2N/Cu(001) the clean Cu(001) surface was sputtered with N_2 for 20 min (flux=100 nA for Cu_2N patches, flux=300 nA for a saturated Cu_2N surface) and annealed for 1 min at 625 K before depositing the KBr(LiCl) again with the sample kept at room temperature and the deposition as described on Cu(001).
The measurements of LiCl were performed at room temperature and at a base pressure in the 1×10^{-10} mbar range with Aahrus SPM, a STM/nc-AFM in Kolibri design. KBr was investigated at the same base pressure, but at 4 K using a Specs JT-STM [10] and an Omicron Nanotechnology LT-STM/AFM with qPlus force sensor[11].
Topographic force and spectroscopy images obtained using STM and AFM were processed using Gwyddion and WSxM[12].

2. Growth of LiCl and KBr on Cu(001) and Cu_2N

Even if LiCl, KBr and Cu_2N are insulators, if they are deposited in ultrathin layers on Cu(001), investigation with STM is possible. If they are thin enough, electrons can tunnel between tip and the conducting sample through the overlaying insulating layer[2]. These properties were used in combination with nc-AFM and allow us to investigate the growth-behaviour of the two rock salt binary compounds.

2.1. Crystal structure of Cu, Cu_2N and rock salt binary compounds

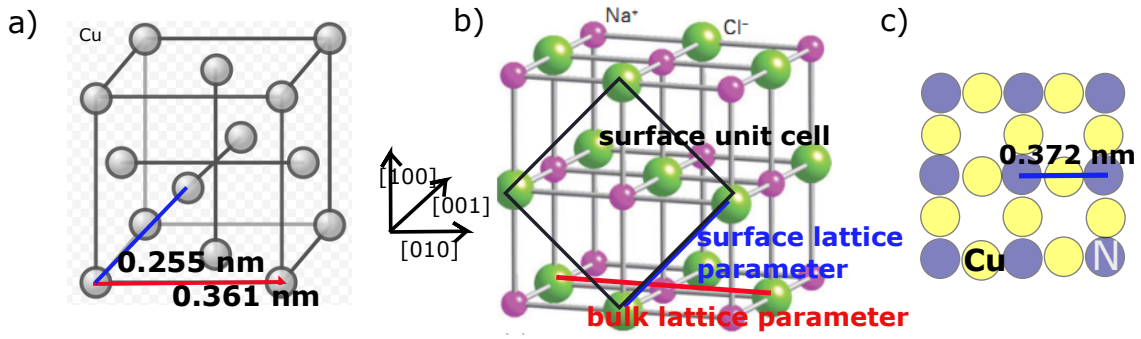

Figure 7: *Crystal structure of Cu and NaCl as example of a rock salt binary compound[13, 14]*

The crystal structure of Cu is face cubic centered (fcc), see fig.7a). The rock salts binary structure LiCl, NaCl and KBr consists of two interleaved fcc-lattices, one of the anions and one of the cations, as shown in fig.7b). The bulk lattice parameters are marked with the red lines. In STM and LEED of the (001) surface, the surface lattice parameter **s** will be measured, which relates to the bulk

lattice parameter **b** as follows:

$$\sqrt{2} = \frac{b}{s} \tag{20}$$

In fig.7c) the structure of Cu_2N is indicated. The surface lattice parameter is 0.372 nm[4].

2.2. Lattice matching of LiCl on Cu(001)

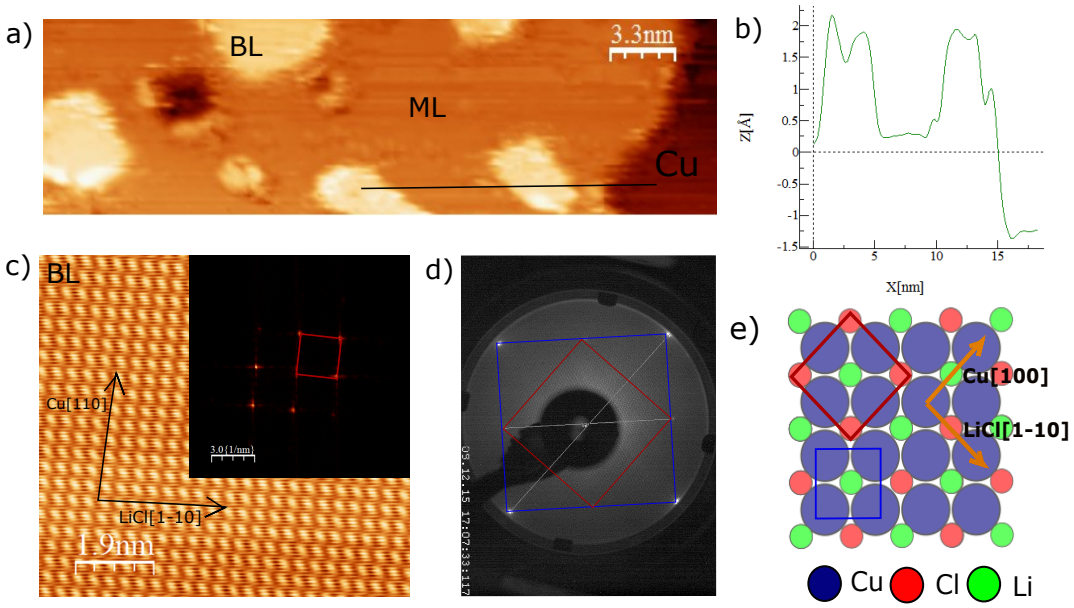

Figure 8: *a) STM topography of LiCl-islands/Cu(001) (V_{bias}=1.18V, I=50pA), b) appearent height profil taken in a), marked with the black line, c) atomic resolution of LiCl-BL and 2D-FFT (V_{bias}=-2.0V, I=30pA), primitive unit cell indicated with red square d) LEED of LiCL/Cu(001): red square primitive unit cell of LiCl, blue square Cu(001), e) schematic top view of LiCL/Cu(001)*

First the gowth of LiCl on Cu(001) was investigated. In fig.8a) a representative overview of a preparation with 20s deposition time of LiCl on Cu(001) is shown: a LiCL-island and supporting smaller LiCl-islands of the next layer. A height profile along the black line is given in fig.8b). At a bias voltage of 1.18V the first layer has an appearent height of 0.15 nm and the second layer of 0.3 nm with respect to the Cu(001) surface. This tridimensional growth with similar step heights for mono- and bilayer has been already reported for other binary rock salts as NaCl and KBr on Cu(001)[1, 17]. We hence conclude that a LiCl-ML-island and small LiCL-BL-island are visible.
A zoom into the LiCl-BL island at V_{bias}=-2 V is shown with atomic resolution in fig.8b). The bright protrusions in the squared pattern are assigned to the Cl-anions analogous to NaCl/Cu(001)[18]. The 2D-FFT transformation, shown as inset in 8c), gives s=(0.365±0.01) nm for the LiCl surface

lattice parameter in the fast scan direction, here the x-direction. (Due to thermal drift, the y-direction are not taken into account.) Simultaneous atomic resolution of Cu(001) and LiCl that is needed for the determination of the surface unit cell could not be archived with STM at room temperature, therefore the growth directions were investigated with LEED as shown in 8c). The red square indicates the primitive unit cell of the deposited LiCl and the blue square the Cu(001) unit cell. With the surface lattice parameter of Cu(001) from literature of s(Cu(001))=0.255 nm[16], the surface lattice parameter of LiCl is calculated to be s(LiCl)=0.362 nm. The difference of the lattice parameters obtained by STM and LEED lies in the range of measuring inaccuracy. For LiCl a surface lattice parameter of 0.362 nm is found in literature[19]. Therefore the measured values are identical to the values from literature, and it is concluded that LiCl keeping its bulk lattice parameter grows as ML-island and BL-island on Cu(001) without sizeable epitaxial strain.
From c) and d) a sketch of the atomic structure of the LiCl-ML was made, shown in 8e). The unit cells in the reciprocal space are indicated as they can be seen in the LEED with a red square for LiCl and a blue square for Cu(001). The cristallographic directions are sketched with orange arrows. The Cu[100]-direction corresponds to the LiCl[110]-direction as also already found in [15]. LiCl grows therefore in a $(\sqrt{2} \times \sqrt{2})$ R45 reconstruction on Cu(001). Li-cations and Cl-anions are placed at the same absorption sites. Due to the lack of simultaneous atomic resolution of LiCl and Cu(001) in our STM measurements we cannot determine the precise adsorption site of the ions. DFT calculations suggests an adsorption on the four-fold hollow site[15].
Due to the lattice matching between Cu(001) and LiCl no strain occurs and also no Moiré or electronic superstructure was observed.

2.3. Strained growth of LiCl on Cu_2N/Cu(001)

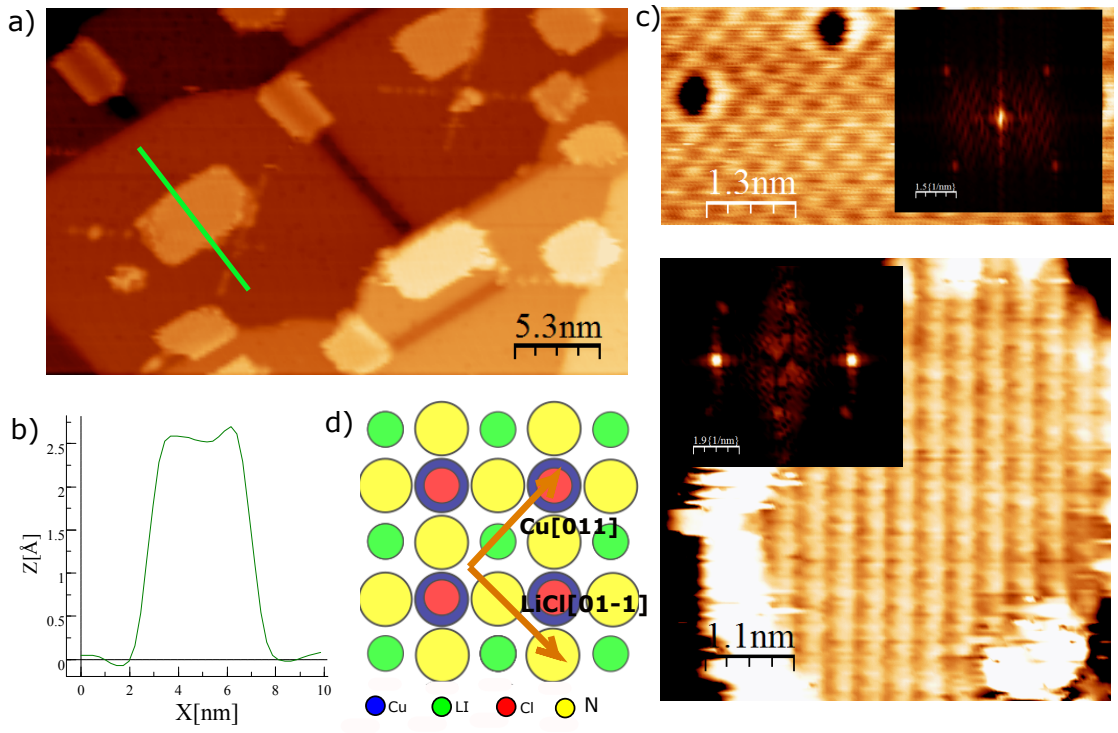

Figure 9: *a) STM topography of LiCl-islands/Cu_2N/Cu(001) (V_{bias}=-2.2V, I=15pA), b) appearent height profile taken in a) indicated with the green line, c) atomic resolution and 2D-FFT of Cu_2N (top, V_{bias}=-2.0V, I=200pA) and LiCl-ML (bottom, V_{bias}=-2.0V, I=40pA), d)schematic top view of LiCL/Cu_2N/Cu(001)*

A topographic overview of a preparation of LiCl on Cu_2N/Cu(001) with a deposition time of 10s is shown in fig.9a). The LiCl-islands grow rectangular with regular borders and overgrow the step edges of Cu_2N smoothly (carpetlike grow). The apparent height at -2 V of the islands with respect to Cu_2N is 0.25 nm, see fig.9b). This is similar to the measured apparent height on NaCl-BL-islands on Cu_2N with 0.265 nm at -1.3V[1] and therefore leads to the conclusion that LiCl-BL-island are visible in fig.9a).

The topographic STM-images with atomic resolution shown in fig.9c) (top: Cu_2N, bottom: LiCl-BL) have been taken subsequently at the same area with the same scanning direction. Surface lattice parameters are obtained with 2D-FFT from this pictures. In the atomic resolution image of Cu_2N at -2V the N-atoms appear as protrusions[16]. The FFTs give surface lattice parameters of (0.37$\pm$0.01) nm for Cu_2N and (0.356$\pm$0.01) nm for LiCl in the fast scan direction, which are identical to the values from literature taken in account errors due to thermal drift and measurement

uncertainties[16]. Here also only the fast scan direction was taken into account for the 2D-FFT. The respective atomic structure of the LiCl-ML on Cu_2N could be sketched, as shown in fig.9d). The Cu[100]-direction of the underlaying substrate corresponds here to the LiCl[100]-direction. The growth direction is identical as found for NaCl/Cu_2N/Cu(001) and also the adsorption site are assumed to be similar[1]. In the range of the measurement uncertainties the surface lattice parameter of LiCl/Cu_2N/Cu(001) and Cu_2N/Cu(001) are identical. No electronical superstructure was observed, therefore we conclude that LiCl/Cu_2N/Cu(001) adopts the surface lattice parameter of Cu_2N/Cu(001) and shows a strain of 2.7%.

2.4. Commensurate growth of KBr on Cu(001)

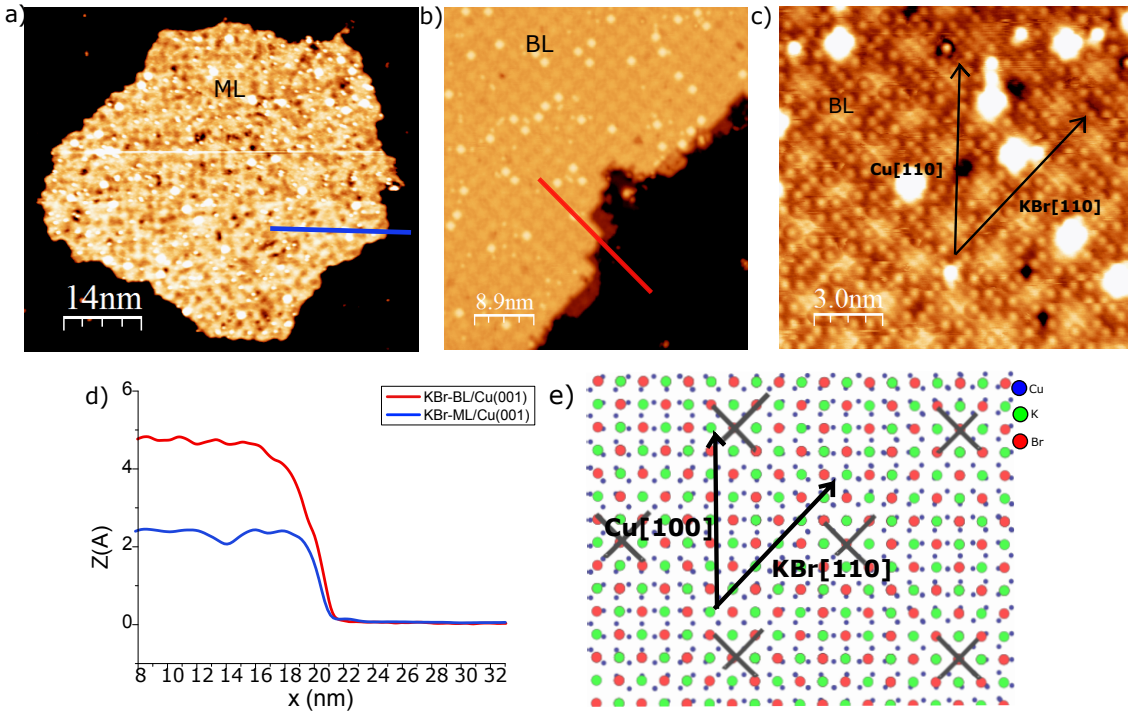

Figure 10: *STM topography of KrB-islands on Cu(001), a) KBr-ML-island (V_{bias}=-1.3 V, I=30pA), b) KBr-BL-island (V_{bias}=-1.3 V, I=15pA), c) Zoom-in with atomic resolution and Moiré of b), d) appearent height profils marked in a) with a blue line and in b) with a red line, e) schematic structure of KBr/Cu(001), the black lines indicate the bright parts in the electronic superstructure*

Several samples of KBr on Cu(001) were prepared at different evaporation rates in order to study the growth on the surface at RT. In fig.10 topographic STM overview of the results of a high

flux preparation (a)) and a low flux preparation (b)) can be found. In a) a KBr-ML- and in b) a KBr-BL-island/Cu(001) are observed as suggested from the appearent height measurements, see 10 d).The appearent heights at -1.3 V for a KBr-ML-island are 0.24 nm and for a KBr-BL-island are 0.48 nm. The height profile trajectories are marked with the blue and red lines in fig.10a) and b). For NaCl-BL/Cu(001) 0.365 nm appearent height at -1.3V was reported, therefore KBr shows a significant higher value[1].
Depending on the coverage, KBr-ML-islands start growing as small islands prefered on step edges, but also on terraces of Cu(001). Higher coverage leads to carpet-like overgrowing the step edges of Cu(001) until forming a closed layer. Carpeliket growth was also reported for NaCl-BL/Cu(001) owing to the low interaction between the Cu(001) surface and NaCl[18]. KBr-BL-islands show a more regular appearence in structure and borders than ML-islands. Small trilayer(TR)-island were observed, but layer-by-layer growth, that occurs in the presence of strong adsorbate-substrate interactions, seems to be prefered over the growth of tridimensional structures as it was also found in [17]. The explanation given there is based on the diatomic molecule character with strong binding of alkali halides and therefore the discussion of their motion in terms of molecular diffusion. The step edges of the BL form a trap for the diffusing KBr molecules, which results in increasing the BL-island and not in forming a TR.
A zoom-in of a KBr-BL-island is shown in fig.10c). The atomic structure and the Moiré are visible. 2D-FFTs gave a surface lattice constant of KBr on Cu(001) of (0.46$\pm$0.01) nm and for the Moiré structure a value of 4.60 nm (10 times the surface lattice parameter). The surface lattice parameter found in literature is 0.461 nm. Therefore also KBr keeps its lattice parameter during the deposition on Cu(001) as LiCl and NaCl. A sketch of the structure as seen in c) can be found in 10e).
The Cu[110]-direction corresponds to the KBr[110]-direction. The black crosses mark the centers of the bright parts of the Moiré structure. A structural Moiré was also observed in an AFM study of KBr/Cu(001) and can hence be attributed to a lattice mismatch of Cu(001) and KBr[17]. From our high resolution STM images (see fig.10) one can see a variation of the atomic structure within the Moiré unit cell. Since this was not present in the reported AFM data[17], its origin is supposed to be rather electronic.

2.5. Strainless growth of KBr on Cu_2N/Cu(001)

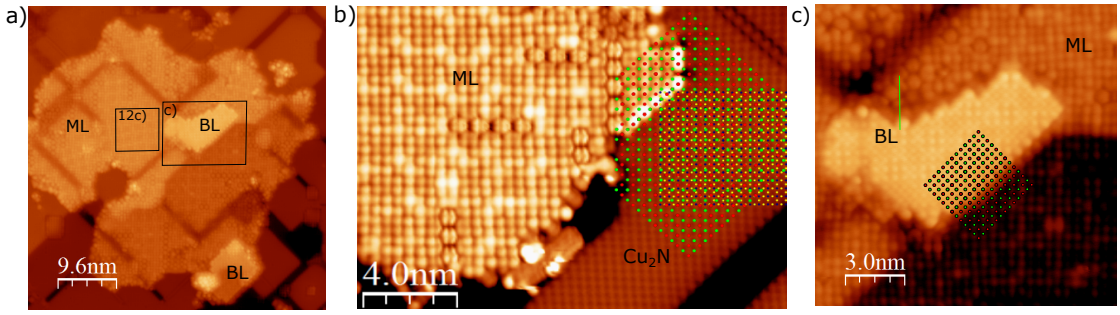

Figure 11: *a) STM topography of KrB-islands on Cu_2N/Cu(001) (V_{bias}=-1.3 V, I=5 pA), b) KBr-ML-island/Cu_2N/Cu(001) and Cu_2N/Cu(001), the lattice of KBr is indicated with red (Br-anions) and green (K-cations) and the lattice of Cu_2N with blue (N) and yellow (Cu) points (V_{bias}=-1.3 V, I=15 pA), c) Zoom in of a) as indicated, the points mark the position of the K-cations (green for BL, red for ML) and the Br-anions (red for BL, green for ML)*

A STM topographic overview can be found in fig.11a): KBr grows carpetlike on Cu_2N/ Cu(001) as ML. BL grows on the top of the ML, but also ML-island completly covered with a second layer are observed. Again the assumption of ML and BL was made with appearent height measurements, the results are shown in table 1 in comparison with NaCl/Cu_2N/Cu(001), both measured at V_{bias}=-1.3 V [1]. As on Cu(001) the structure of the BL is more regular than the ML one. In contrast

Table 1: *Appearent height measurements of KBr and NaCl/Cu_2N/Cu(001) at V_{bias}=-1.3 V*

	height ML [nm]	height BL [nm]
KBr	0.28	0.49
NaCl[18]	0.315	0.535

to NaCl and LiCl, in KBr/Cu_2N/Cu(001) no crystallographic direction seems to be preferred. Therefore also different types of the superstructure are observed.
In fig.11b) a KBr-ML-island on Cu_2 N is shown, the atomic structure of both materials is indicated with points again. The blue points correspond to N-atoms, the yellow ones to the Cu-atoms. A zoom in of fig.11a) is shown in fig.11c). The red and the green points indicate the position of the Br- and K-atoms, respectively. In the ML, the colors are reversed, which leads to the conclusion that the K-cations of the BL adsorbs on a Br-anions of a ML and vise versa. Therefore it grows in the same structure as in bulk, see fig.7b).
A schematic top view of KBr/Cu_2N is sketched in fig.12. The bright parts of the superstructure are marked with black lines. In fig.12b) and c) two different superstructures rotated by 8 degrees

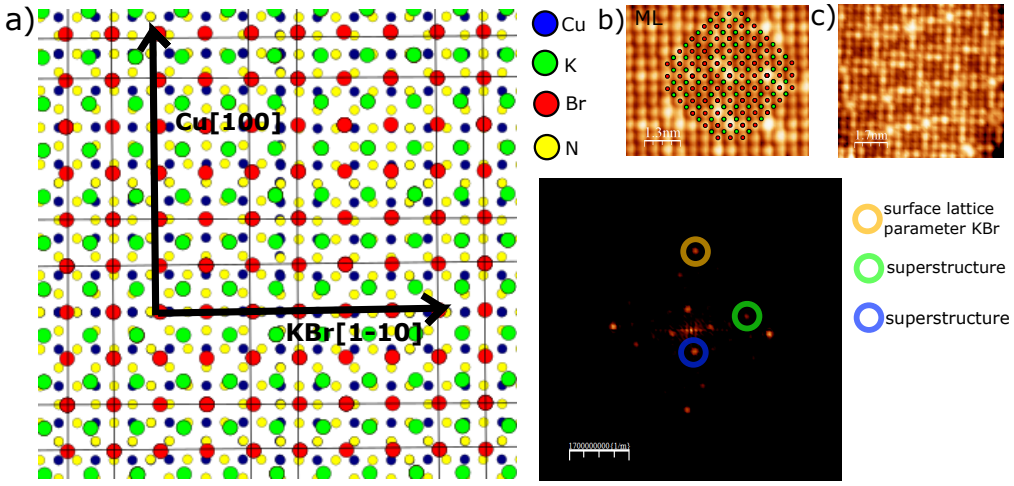

Figure 12: *a)schematic top view of KBr/Cu_2N/ Cu(001) with growth Cu[100]||KBr[110] as in fig.11c), b) atomic resolution of KBr-ML/Cu_2N/ Cu(001): only the red marked Br-anions are visible in the STM topography (green K-cations)(V_{bias}=-1.3 V, I=15 pA), c)atmic resolution of a different superstructure as in b) and 2D-FFT, the primitive unit cell of KBr and two periodicities of the superstructure can be found (V_{bias}=-1.3 V, I=15 pA)*

with atomic resolution of KBr-ML-islands are shown. Only the Br-anions are visible in the atomic resolution. The 2D-FFT of the STM topography in fig.12c) of the also in c) shown superstructure gives three unit cells: the primitive unit cell of KBr and two unit cells corresponding to the superstructure. The surface lattice parameter was found to be 0.455 nm, the superstructure parameter to be 1.66 nm. The superstructure contains a subsuperstructure with parameter of 0.6 nm. The surface lattice parameter is similar to the one from literature.

An investigation of the electronic structure of the bilayer in comparison with the topographic

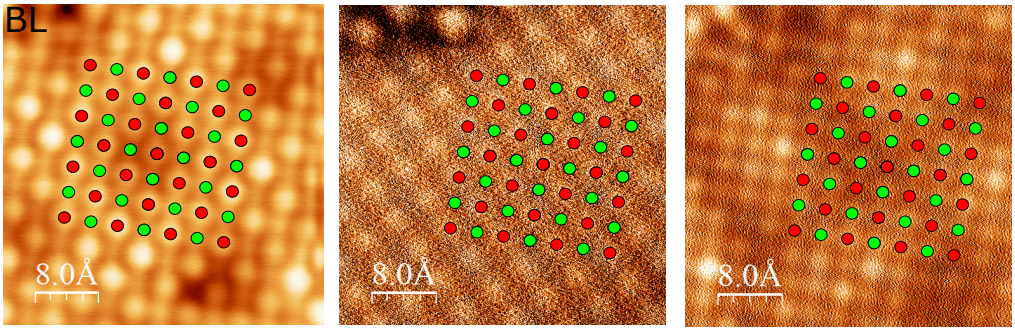

Figure 13: *KBr-BL/Cu_2N zoom-in STM topography (constant current, V_{bias}=-1.3V, I=30pA), force map (constant height, feedback opened at V_{bias}=-1.3V, I=30pA, z-offset=-0.14 pm), STM topography (constant height, feedback opened at V_{bias}=-1.3V, I=30pA, z-offset=-0.14 pm), simultaneous taken with force map)*

structure can be found in fig.13. From left to right a STM topography taken constant current, a force map and a simultaneous tunneling current taken in constant height mode is shown. Again the Br-anion and the K-cations are indicated. Therefore unlike in the ML, in the BL both types of atoms are visible with STM. With AFM only the Br-anions are observed. Also the superstructure is missing in the AFM topography, with leads to the conclusion that it is only electronic.

3. Electronic properties

After describing the growth behaviour of KBr on Cu(001) and Cu_2N/Cu(001), the following section will shown the electronic properties especially in order to elucidate how the Moiré structure influences the electronic properties of the ad-layer.

3.1. Workfunctions

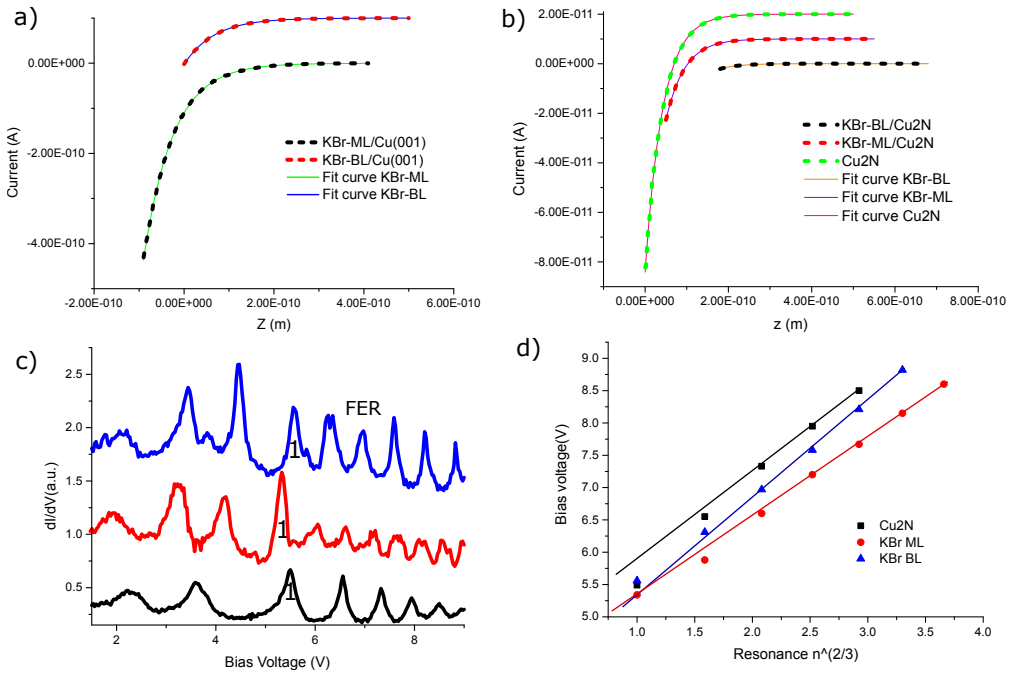

Figure 14: *Calculation of the work functions of the different surfaces: a) I(z)-spectroscopy of KBr/Cu(001) (setpoint: V_{bias}=-1.3V, I=100pA), b) I(z)-spectroscopy of KBr/Cu_2N/Cu(001) (setpoint: V_{bias}=-1.3V, I=100pA), both with exponential fits for the calculation of the workfunctions ϕ, see eq. (2) and (3), c) STS measurements at KBr/Cu_2N/Cu(001) and Cu_2N/Cu(001) (V_{bias}=3 V, I=25 pA), d) peak voltages of the FER resonances plotted against the resonance numbers, the intersect with the y-axis of the indicated linear fits give workfunctions ϕ, see eq.(5)*

Table 2: *Workfunction measurements with I(z)-spectroscopy and FER on Cu_2N and KBr-ML/BL-islands/Cu(001) and on Cu_2N/Cu(001)*

	ϕ(Cu_2N) [eV]	ϕ(KBr-ML/Cu_2N) [eV]	ϕ(KBr-BL/Cu_2N) [eV]
I(z)-spectroscopy	(5.0±0.8)	(4.9±0.7)	(4.1±0.7)
FER	(4.4±0.2)	(4.0±0.2)	(3.8±0.2)

	ϕ(KBr-ML/Cu(001)) [eV]	ϕ(KBr-BL/Cu(001)) [eV]
I(z)-spectroscopy	(2.1±0.2)	(2.0±0.1)

Fig.14a) and b) show I(z)-spectroscopy data of KBr-ML and KBr-BL on Cu(001) and on Cu_2N, respectively. The different z-scan ranges have been selected to guarantee that the tip apex is always at the same distance from the surface atoms, so that structural distortions upon tip approach can be disregarded. The exponential fits are also marked in the graphs. From these fits the work functions are calculated with eq.(1) and (2) and summarized in table 2.
FER measurements are shown in fig.14c). In fig.14d) the peak positions are plotted against the resonance numbers $n^{2/3}$. The result was fitted with a linear function, where the first two peaks are neglected[20]. The intersect with the y-axis yields the workfunction, see section 2.6.3 and eq.(6). At closed feedback, the tip will be continuously retracted with increasing voltage, therefore **E**=V/z is assumed to be constant. The results are shown in table 2.
The workfunction difference found in [17] are 1.1eV/1.3eV between Cu(001) and ML/BL-island measured with Kelvin-Probe. Extracted work functions from the I(z)-curves in fig.14a), show also a clearly decrease of the workfunction from ML- and to BL-islands, therefore these two methods give the same tendency. The decrease found between Cu_2N and KBr-ML/Cu_2N/Cu(001) and KBr-BL/Cu_2N is 0.1 eV/0.9 eV (I(z)-spectroscopy)) and 0.4 eV/0.6 eV (FER). More importantly the work function is clearly larger than on KBr/Cu(001). In Cu_2N, the dipole created at the metal surface is much smaller than in bare Cu(001), and this avoids the quenching of the dipole occuring at the interface of polar materials with metallic electrodes. This has profound consequences in the stabilization of electric polarization in the ultrathin regime[25].

3.2. Structural Moiré induced electronic superstructure of KBr/Cu(001)

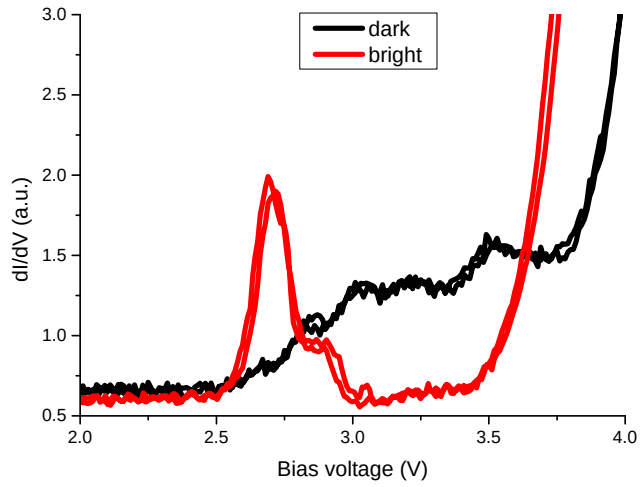

Figure 15: *STS on KBr-BL-island on bright and dark spots of the superstructure shown in fig.16 at 2.7V (feedback opened at V_{bias}=3.0V, I=50pA)*

For the investigation of the electronic structure of KBr/Cu(001), we conducted spatially resolved dI/dV-spectroscopy, see fig.15, and STM topographies at different bias voltages, see fig.16. As shown in fig.15 the conduction band edge is found site dependend between 3.7V and 4V for BL-islands, depending on the selected position in the superstructure. Due to the deposition of KBr-BL on Cu(001) in-gap-states are formed. Peaks are found at 2.7V, 2.9V, 3.0V, 3.2V and 3.5V, see fig.15. To display the site dependence of the electronic density of states as a function of the bias voltage, STM topographies at the bias voltages showing peaks in the STS were taken. These topographies are shown in fig.16. The local character of the electronic states is clearly visible. We have performed

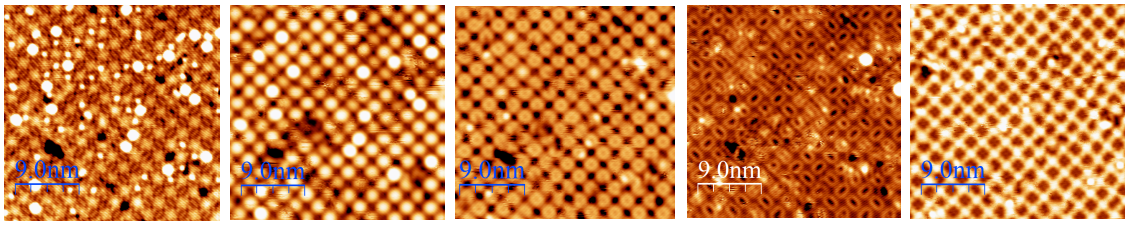

Figure 16: *STM topography at different bias voltages of KBr-BL-island on Cu(001) from left to right: V_{bias}=-1.0V, I=50pA; V_{bias}=2.7 V, I=50pA; V_{bias}=3.0 V, I=50pA; V_{bias}=3.2V, I=50pA; V_{bias}=3.5V, I=50pA*

analogue measurements on the KBr-ML/Cu(001) as shown in fig.17. The conduction band edge is lowered in this case to 3.5V. The in-gap states are found at the same bias voltages as for the KBr-BL, see fig.17a). In fig.17b) several dI/dV-maps and a topographic overview over the same area are shown. Also here the electronic states which are found in the STS show a local character. The appearence of a electronic superstructure that resembles the structural Moiré can be caused by the change of the work function due to the different distances between the atoms of the Cu(001)

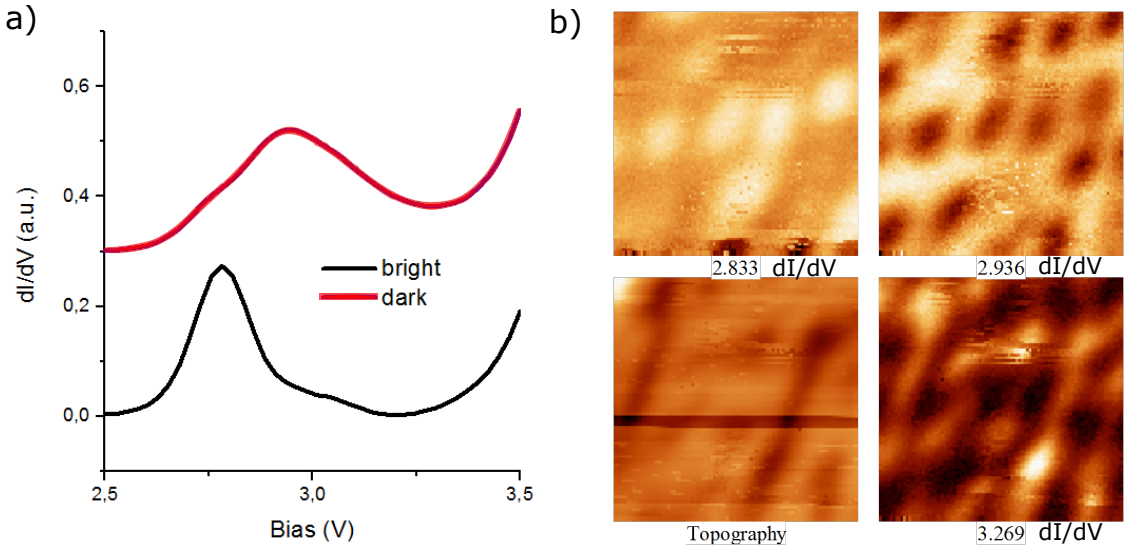

Figure 17: *dI/dV measurements on KBr/Cu(001) a) STS on KBr-ML-islands (feedback opened at V_{bias}=3.0V, I=15pA) b) different dI/dV-maps and STM topography taken at the same spot of a KBr-ML-island (topography constant height, setpoint V_{bias}=3.0, I=15pA, dI/dV-maps from grid-spectroscopy, see a))*

and the adsorbed KBr-molecules in the z-direction. At first approximation periodic variation of the surface-adatom distance cause a modulation of the surface image potentials and leads therefore to a site dependence of the workfunctions[21].

The in-gap states appear due to the hybridization of KBr with Cu(001), which enable the appearence of states also inside the band gap of the insulator. Therefore they are already observed in the ML and an additional coverage does not influence them. This is the typical behaviour of a surface resonance vertically located between the last Cu layer and the first KBr layer.

3.3. The influence of Cu_2N on the electronic structure

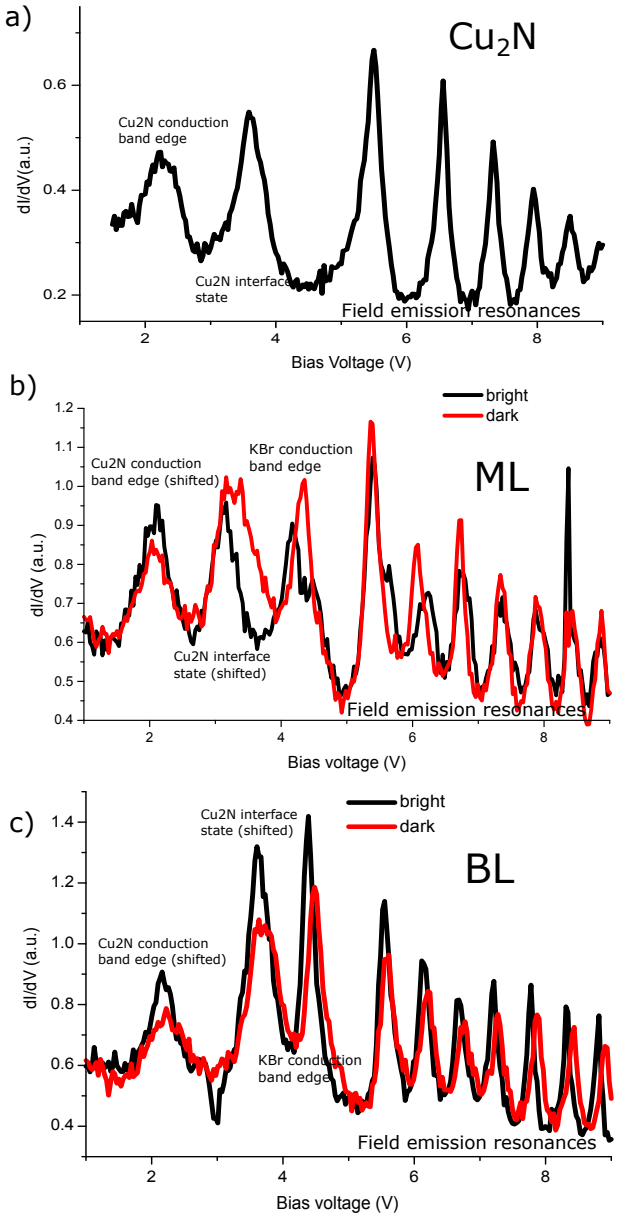

Figure 18: *FER measurements a) KBr-ML-island/Cu_2N/Cu(001), b) KBr-ML-island/Cu_2N/Cu(001) and c) KBr-BL-island/Cu_2N/Cu(001) (all closed feedback, V_{bias}=3V, I=25 pA)*

In fig.18 closed-feedback dI/dV spectra are shown in an ample voltage range measured on different surface areas with the same tip. In fig.18a) the Cu_2N conduction band edge (at 2.2 eV) and the interface state as well the FER occuring on Cu_2N/Cu(001) are visible and indicated. The corresponding spectra on different sites of a KBr-ML-island/Cu_2N/Cu(001) are shown in fig.18b). The red graph corresponds to a measurement in a dark spot of the electronic superstructure and the black one to a bright spot. On the KBr-ML-island the Cu_2N conduction band edge appears shifted to 2 eV. The Cu_2N/Cu(001) interface state is also shifted in comparison to the bare Cu_2N[8]. Since KBr is not in contact with the Cu surface, no in-gap states are found.

Corresponding STS spectroscopy at a KBr-BL-island /Cu_2N/Cu(001) is shown in fig.18c), there the conducting band edges and the interface state of Cu_2N/Cu(001) are shifted to higher energies with respect to the STS measurements at the KBr-ML. As for the ML, also here no in-gap states were observed.

As can be seen in fig.19a), the Cu_2N interface state shifts clearly depending on the measurement spot owing to the electronic superstructure. It can be observed, that the peak changes from 3.3V to 3.7V while going from a bright spot to a dark spot of the superstructure. In contrast,

STS of the BL shown in fig.19b) in the range up to 3.7 V is homogeneous because the Cu_2N/Cu(001) interface state is located at higher energies.
In fig.19c) and d) the peak position of the FERs are plottet against the resonance numbers $n^{2/3}$. Linear fits neglecting the first two FER resonances show for that the work function of a bright spot is lower than that of a dark spot on ML- and BL-islands, see table3. This is also reported for

Table 3: *Workfunction measurements with FER on Cu_2N and KBr-ML/BL-islands*

	ϕ(KBr-ML/Cu_2N) [eV]	ϕ(KBr-BL/Cu_2N) [eV]
bright	(3.92±0.1)	(3.82±0.1)
dark	(3.98±0.1)	(3.86±0.1)

NaCl/Ag(001)[21].
The FER resonances are assumed to be influenced by the image potentials of the surface, which

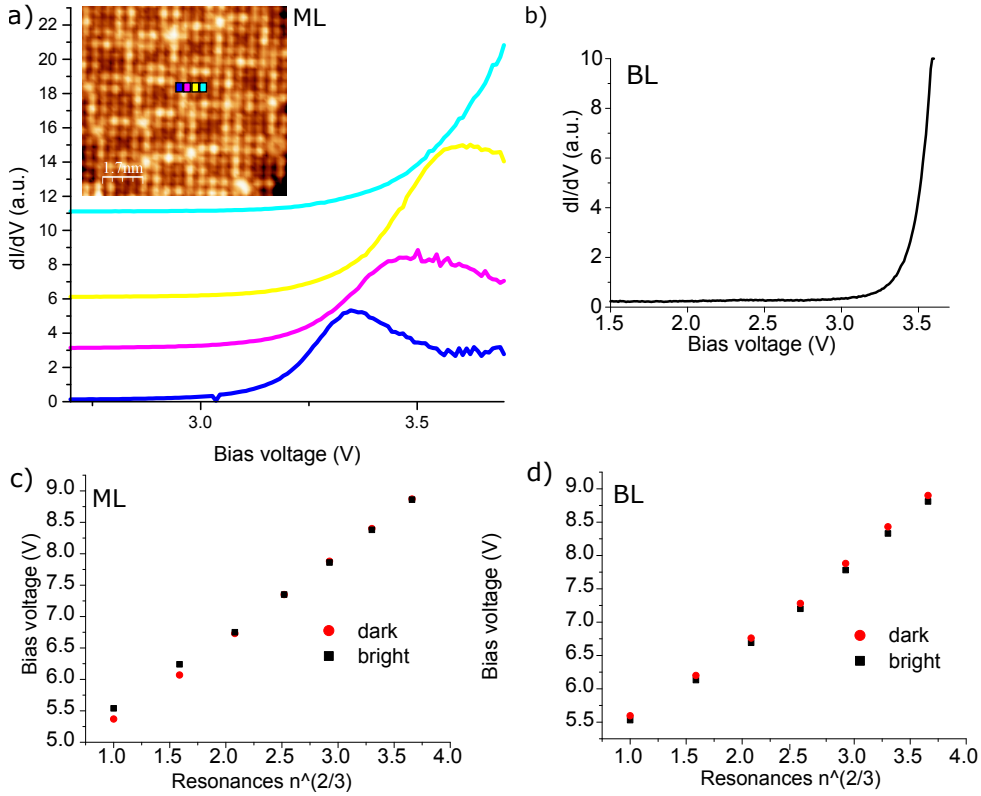

Figure 19: *a) STS measurements, measurement positions indicated in the inset: atomic resolution of KBr-ML/Cu_2N/Cu(001) (V_{bias}=-1.3V, I=15pA), (constant height, setpoint: V_{bias}=3V, I=15pA), b) STS-curve measured on KBr-BL/Cu_2N/Cu(001), (constant height, setpoint: V_{bias}=3V, I=15pA), c) and d) analysis of the peak bias voltages in dependence of the resonance number, see fig.18*

forms unoccupied states bound by the image charge response of the Cu(001)-surface. For KBr-

ML-island/Cu_2N/Cu(001) also a structural Moiré could be the possible origin as in the case of NaCl/Ag(001) and KBr/Cu(001). But as shown for the KBr-BL on Cu_2N (fig.13), no strain and no structural Moiré are necessary for the appearence of the electronic superstructure.
It can be concluded that, due to the spacing insulator Cu_2N, the hybridization between KBr and Cu(001) disappears. Therefore the in-gap-states due to hybridization mentioned in section 3.2 also disappear. The observed states in the STS measurements in the band gap of KBr taken at KBr/Cu_2N/Cu(001) come from Cu_2N/Cu(001). The conduction band edge and the interface state of Cu_2N are visible. The interface state is shifted in the KBr-ML due to the changes in the induced dipole across the different positions of the electronic superstructure. In the KBr-BL the superstructure does not have any influence on the Cu_2N interface state position.

4. Ferroelectric effects in KBr-BL-islands/Cu_2N/Cu(001)

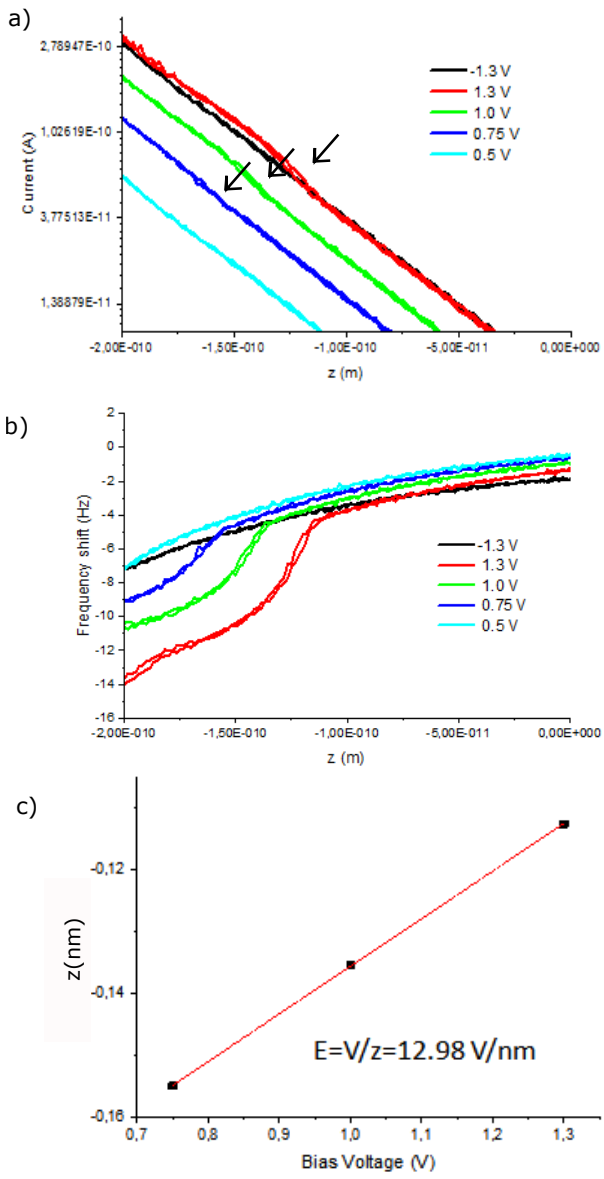

Figure 20: *a)I(z)-spectroscopy on KBr-BL/Cu_2N/Cu(001), (setpoint: V_{bias}=-1.3V, I=50pA), b) simultaneous to a) taken Δ f(z)-spectroscopy, c)z_c, at which the transitions in a) and b) occur, plottet against $V_b$ias and linear fitted, slope of the fit equal the electrical field E=V/z*

For NaCl-Bl/Cu_2N/Cu(001) an electric field induced switching of two different polarization states was reported (see fig.1)[2]. Intriguinly, similar ferroelectric effects in KBr-BL-island/Cu_2N /Cu(001) can be observed in I(z)-, Δf(z)-, I(V)- and Δf(V)-spectroscopy.

Fig.20a) and b) shows Δf(z)- and I(z)-curves taken simultaneously. In fig.20a) I(z)-spectroscopy data at different bias voltages V_{bias} is shown. For a positive sample bias above 0.75 V a transition in form of a step in the current can be observed. At both sides of the transition the current follows an exponential decay with very similar workfunction. Due to the relation **E**=V/z, a variation of the bias voltage V_{bias} with a constant height z or a variation of z with V_{bias} constant should cause a transition in the previous mentioned spectroscopy methods, when a certain value for the electric field is matched. The I(z)-curves the step appears due to a change in the workfunction of the surface (see eq.(1) and (2)), which is proportional to the surface dipole. Therefore the tunneling current changes when the dipole is switched, see section 2.4 and 2.7. In the Δf(z)-curves shown in fig.20b) for the same bias voltages as in the I(z)-

curves and at the same critical height z_c, a sharp drop of the frequency shift Δf(z) is visible. The origin of this feature is the change of the dipole-related electrostatic force, as reported for $NaCl/Cu_2N/Cu(001)$[1]. In fig.20c) z_c is plotted against the bias voltages of the curves with transitions, confirming the linear relationship between z_c and V_c characteristic of an electric field driven process. For this tip an electric field of 13 V/nm is derived from the slope and it allowed no observation of a hysteresis cycle.

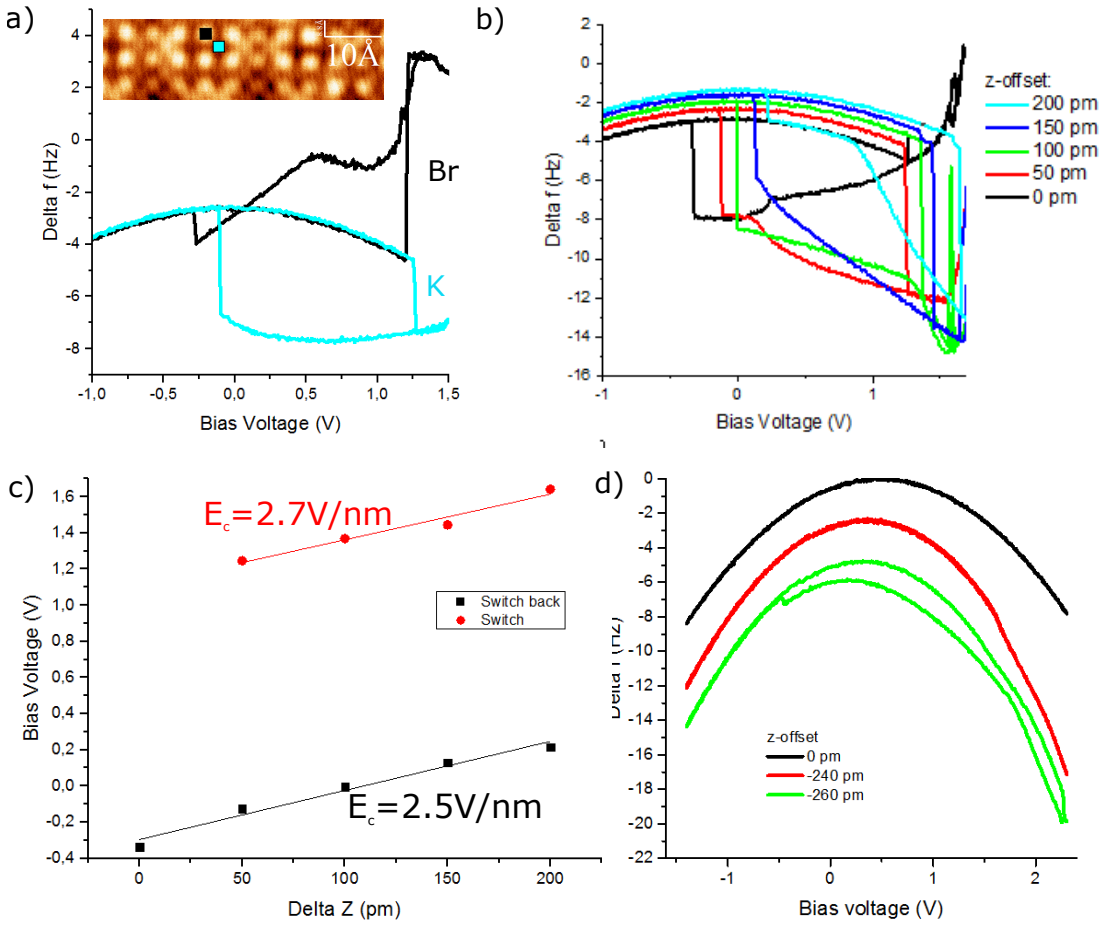

Figure 21: *Ferroelectric effect in Δf(V)-measurements on KBr-BL/Cu_2N/Cu(001) a) Δf(V)-spectroscopy, spectroscopy locations indicated in the STM topography inset (topography and spectroscopy setpoint: V_{bias}=-1.3V, I=5pA) b) Δf(V)-spectroscopy at different z-offsets c) z_c, at which the switch and the back-switch in b) occur, plottet against $V_b$ias and linear fitted, d)Δf(V)-spectroscopy at diffenrent z-offsets with a different tip in comparison to a) and b)(setpoint:V_{bias}=-1.3V, I=5pA)*

The transitions between different polarization states as seen in Δf(V)-spectroscopy are shown in fig.21a), b) and c). In most of the cases a hysteresis can be observed. In fig.21a) the dependence of the measuring spot is indicated. The black curve corresponds to the measurement on a Br-anions,

the blue one is taken on top of a K-cation. The black curve shifts after the transition to smaller Δf(V)-values, which leads to the conclusion that the chemical interaction with Br-anion decreases due to a displacement in z direction (further from the tip). The blue curve instead changes to higher Δf(V)-values, which leads to the opposite conclusion: a position change in positive direction (closer to the tip). This process would therefore be analog to the transition of the position of anion and cation found for NaCl-BL/Cu_2N/Cu(001). The observed transition in the Δf(V)-spectroscopy is not only dependent on the position on top the anion or cation, but also on the measurement position relative to the superstructure. In fig.21b) the height dependence of the hysteresis is shown. The critical bias voltage V_c, where the coercive electric fields of the hysteresis occurs as a function of the z-offset can be found in fig.21c). Again the electrical field was calculated and a value of 2.7 V/nm for the switch and a value of 2.5 V/nm for the back-switch were found. The appearence and the form of the hysteresis depends not only on the measurement position within the unit cell of the superstructure, but also on the shape of the tip. The measurements in b) and d) are taken with the same setpoint of V_{bias}=-1.3V, I=5pA, but using tips with different termination. The hysteresis in b) occurs already as far as with a z-offset of 200 pm measured from the regulation distance, while in d) a decrease of the tip-sample distance of -240 pm causes only a transition at around 1.7 V and at -260 pm a hysteresis can be observed. The electrical fields, measured with this second tip, are 6 V/nm for the switch and -2 V/nm for the back-switch.

The behaviour of the electric polarization found for KBr-BL/Cu_2N/Cu(001) is quite similar to the behaviour of NaCl-BL/Cu_2N/Cu(001) with the difference, that the hysteresis only appears for NaCl-BL/Cu_2N/Cu(001) around vacancies. In the KBr case the electronic superstructure could be consider as a periodic defect pattern, mirroting the role of vacancies in NaCl. The different adsorbing positions of the KBr-molecules with respect to the Cu_2N-lattice could be assumed to have the character of defects.

Also it was found that for some tips the back-switch voltage does not approach the switch voltage as it is the case for NaCl (fig.21c). This leads to the conclusion that the model of a parallel plane capacitor for the tip-sample system is not sufficient to describe the electrostatic potential at the KBr film. Therefore atomistic details of the tip apex and the electronic superstructure have to be taken into account.

Summary

The aim of this work was the characterization of two different rock salt binary compounds, LiCl and KBr, on Cu(001) and Cu_2N/Cu(001) with respect to their growth behaviour, their electronic properties and the electrostatic interactions with Cu_2N/Cu(001). In particular, the last point motivated the investigation because of the observed piezoelectric and ferroelectric effects of NaCl-BL/Cu_2N/Cu(001).

The assumed origin of the piezo-/ferroelectric behaviour of NaCl-BL/Cu_2N/Cu(001) was the occuring strain. Therefore LiCl, whose lattice constant matchs quite well with the ones of Cu(001) and Cu_2N/Cu(001) was investigated with STM and LEED only with respect to the growth behaviour at room temperature. The results found, are similar to NaCl with the difference that on Cu(001) also LiCl-ML could be observed, while for NaCl only BL and higher layers grew. On Cu_2N a strain of 2.7% can be found. The electric polarization of this material will be investigated in the future.

After this investigation, KBr was deposited on the two mentioned surfaces. The growth behaviour is also quite similar to the other binary rock salts on Cu(001). However, in sharp contrast, on Cu_2N/Cu(001) no strain occurs. Still ferroelectric effects were observed for KBr-BL/Cu_2N /Cu(001). Therefore the strain does not seem to be the key parameter in this phenomenon. While the discontinuous switching of the polarization resembles that of NaCl in all aspects, the hysteretical behaviour seems to depend on the adsorption sites of KBr with respect to Cu_2N/Cu(001). This suggests that, rather than epitaxial strain, electronic decoupling and breaking of the inversion symmetry introduced by the polar Cu_2N surface are the key ingredients to turn a regular ionic rocksalt into an ultrathin ferroelectric film.

Besides this result, whose origin needs more investigation, also interesting electronic properties of KBr/Cu(001) and KBr/Cu_2N/Cu(001) could be observed. A periodic electronic superstructure occurs in both systems. This superstructure can be related to changes in the workfunction, which are assumed to be caused for KBr/Cu(001) by the image potential differences due to the variation of the interatomic distances arising from the structural Moiré. The AFM measurements indicate that for KBr/Cu_2N different adsorption sites are the reason, rather than a structural Moiré.

The contrast the superstructure is found to be bias dependent in the STM topography and dI/dV measurements. STS measurements show states at lower bias voltages than the conduction band edge of KBr for all systems, but with different origins: the electronic hybridization between Cu(001) and KBr is suppressed by the 1 ML thick Cu_2N spacer.

In conclusion is can be said, that the KBr-BL/Cu_2N/Cu(001) is a promising system for ferroelectronics, because also a defect-free BL and not only at vacancies as for NaCl-BL/Cu_2N/Cu(001) switchable polarization states could be found.

References

[1] J. Martinez Castro. Atomically Thin Stacks of Polar Insulators: A Route to Atomic-Scale Multiferroics. PhD thesis. Department of Physics and Astronomy. University of London. 2016

[2] J. Martinez-Castro et al. Electric-field-induced reversal of teh spontaneous polarization in an atomically thin ionic insulator. Soon to be published.

[3] C. Lotze. Fundamental Processes in Single Molecule Junctions: Interplay of Forces and Electronic Effects. PhD thesis. FU Berlin. 2013

[4] G.Schulze. Elementary Processes in Signal Molecule Devices: Electronic Transport and Molecular Isomerization. PhD thesis. FU Berlin. 2009

[5] W. Demtröder. Experimentalphysik 2. Springer-Lehrbuch (Springer Berlin Heidelberg, Berlin, Heidelberg). 2009

[6] H. Hamaker. The London-van der Waals attraction between spherical particles. Physica 4 (1058). 1937

[7] T.C. Leung et al. Relationship between surface dipole, work function and charge transfer: Some exceptions to an established rule. Phys. Rev. B 68 (195408). 2003

[8] T.König et al., Work Function Measurements of Thin Oxide Films on Metals-MgO on Ag(001), J.Phys.Chem. C 113 (11301). 2009

[9] Lexikon der Physik: elektrische Polarisation, Spektrum der Wissenschaft. 22.08.2016

[10] L. Zhang et al. A compact sub-Kelvin ultrahigh vacuum scanning tunneling miscroscope with high energy resolution and high stability. Rev. Sci. Instrum. 82 (103702). 2011

[11] F. Giessibl et al. High-speed force sensor for force miscroscopy and profilometry utilizing a quartz tuning fork. Appl. Phys. Lett. 73 (3956). 1998

[12] I. Horcas et al. WSXM: A software for scanning probe microscopy and a tool for nanotechnology. Rev. Sci. Instrum. 78 (013705). 2007

[13] M.Kiguchi et al. Heteroepitaxial growth of LiCl on Cu(001). Phys. Rev. B. 63 (205418). 2001

[14] Fcc-lattice Cu

[15] Crystal structure rock salt binary compounds

[16] T.Choi et al. Incommensurability and atomic structure of c(2×2)N/Cu(001): A scanning tunneling microscopy study. Phys. Rev. B 78 (035430). 2008

[17] T. Filleter et al., Atomic structure and friction of ultrathin films of KBr on Cu(001), Phys.Rev. B 77 (035430). 2008

[18] Q.Guo et al. Bias dependence of apparent layer thickness and Moiré pattern on NaCl/Cu(001). Surf. Sci. 604 (1820). 2010

[19] Lattice parameter LiCl. 13.08.2016

[20] G.Binnig et al. Tunneling Spectroscopy and Inverse Photoemission: Image and Field states. Phys. Rev. Lett. 55 (991). 1985

[21] M.Pivetta et al. Local work function Moiré pattern on ultrathin ionic films: NaCl on Ag(100). Phys. Rev. B 72 (115404). 2005

[22] C.D.Ruggiero et al. Emergence of surface states in nanoscale Cu2N islands, Phys. Rev. B 83, 245430, 2011

[23] J.Tersoff and D.R. Hamann. Theory and Application for the Scanning Tunneling Microscope. Phys. Rev. Lett. 50 (1998). 1983

[24] S.Sadewasser et al. New Insights on Atomic-Resolution Frequency-Modulation Kelvin-Probe Force-Microscopy Imaging of Semiconductors. Phys. Rev. Lett. 103(266103). 2009

[25] M.Stengel et al. Enhancement of ferroelectricity at metal-oxide interfaces. Nat. Mat. 8 (392). 2009

Acknowledgements

First I would like to thank Prof. David Serrate for the oportunity to write my master thesis in his group and offer me the information about the scholarship of the Fundación INA.
Thanks also to Marten, Carlos and Jose! Thank you for all the advices, explanations, the patience and all the support especially at the beginning, when I had a lot of troubles with the language. I felt really welcomed in your group and it was a pleasure working with you.
You already know that I am not a person who speaks a lot, but really, thank you for all!